PROLIFIC APPLICATION OF GREEN SYNTHESISED CdS NANOPARTICLES FOR THE SEQUESTRATION OF CATIONIC DYES FROM AQUEOUS SOLUTION

G. Tamil Elakkiya[1], G. Sundararajan[1*], R. Lakshmipathy[2], P. Anitha[3] and N. Muruganantham[1]

[1]Department of Chemistry, Thanthai Hans Roever College (Autonomous), Perambalur-621220 (Affiliated to Bharathidasan University, Tiruchirappalli), Tamil Nadu, India
[2]Directorate of Learning and Development, SRM Institute of Science and Technology, Kattankulathur, Tamil Nadu, India – 603203
[3]Department of Physics, SRM TRP Engineering College (Affiliated to Anna University), Tiruchirapalli, Tamil Nadu, India

ABSTRACT. Synthesis of cadmium sulfide (CdS) nanoparticles using watermelon rind aqueous extract was explored for its effectiveness in eliminating Methylene Blue (MB) and Crystal Violet (CV) dyes from water. The synthesised CdS nanoparticles were characterised with XRD, TEM and EDX and found to be around 10 nm in size with spherical shape. A central composite design was developed to optimise independent variables such as pH, contact time and initial concentrations. The developed quadratic model was found to be significant with p-value <0.0001 and lack of fit >0.005 suggesting the reliability of the model. Isotherm modelling analysis revealed that Langmuir and Freundlich's isotherms provided better explanation for the equilibrium data. The loading capacities of the CdS nanoparticles were found be 227.3 and 185.1 mg g^{-1}, respectively for MB and CV. The experimental data showed a good fit with the pseudo-second-order kinetic model, indicating that chemical reactions were the determining factor in controlling the rate-limiting step. Thermodynamic analyses indicated that the process was spontaneous and exothermic. Desorption and regeneration investigations demonstrated that CdS nanoparticles could be successfully regenerated up to 5 times and reused in the adsorption process. The results conclude that the CdS nanoparticles are capable of remediating water containing cationic dyes.

KEY WORDS: Watermelon rind, CdS nanoparticles, Synthetic dyes, Adsorption, RSM

INTRODUCTION

Synthetic dyes play a crucial role in diverse industries such as textiles, garments, and food production [1]. Their widespread use in the textile industry results in colored dye content in textile effluents [2]. This colored wastewater poses a threat to water streams and ecosystems, adversely impacting aquatic life and species [3]. The synthetic dyes affect the aquatic ecosystems and destroy the phytoplankton and zooplankton. Therefore, it is imperative to treat colored water before its release into the ecosystem. Methylene Blue and Crystal Violet dyes are extensively used in the dyeing industries and are released in large quantities in to the water streams and hence they are targeted by majority of researchers. Numerous treatment methods are available for managing and remediating inorganic species in water streams, with adsorption being recognized as a highly promising technique [5]. Adsorption is superior just due to being eco-friendly and economical in the process. Various adsorbents, including activated carbon [6], agricultural residues [7], industrial by-products [8], zeolites [9], and nanomaterials [10], have been explored for the removal of heavy metal ions from aqueous environments. Nanomaterials exhibit great promise as adsorbents for heavy metal ion removal due to their high efficiency, substantial adsorption capacity, and excellent regeneration capability [11].

Considering the superiority of the nanomaterials, a variety of nanomaterials and nanocomposites were applied in the removal of heavy metal ions and synthetic dyes from aqueous

_____

solutions. Magnetic nanorods were efficiently used to remove 6 heavy metal ions from aqueous solution with superior capacity [12]. Platinum doped titanate nanomaterial was successfully as an adsorbent and photocatalyst towards cationic and anionic dyes and the adsorption and degradation was pronounced for cationic dyes [13]. MgO nanoparticles were employed in the adsorption of Remazol Red BB-133 dye from aqueous solution [14]. A nano-organic framework incorporating ZnO nanomaterials was employed to eliminate Malachite Green dye from aqueous solutions, demonstrating superior efficiency compared to several other adsorbents [15]. Titanium dioxide nanoparticles, in conjunction with MWCTs, were applied for removing fuchsine blue dye from aqueous solutions [16]. Additionally, green-synthesized Iron nanoparticles, featuring polyphenols on their surface, were employed for the removal of fluoride and methylene blue dye [17].

While there are limited reports on ZnO, TiO, MgO and CuO nano adsorbents, information on CdS nanomaterials as adsorbents is notably lacking to the best of our knowledge. In consideration of this, CdS nanoparticles, previously synthesized using watermelon rind aqueous extract [18], were investigated for their efficacy in removing Methylene blue and Crystal Violet from aqueous solutions.

EXPERIMENTAL

Synthesis of CdS nanoparticles

Watermelon rind was initially air and oven dried pieces and later 2 g were added to 150 mL of distilled water present in a beaker. The mixture was heated for about 30 min with continuous stirring on a magnetic stirrer at 70 ºC and the heated mixture was brought down to room temperature. The cooled mixture was subjected to filtration in order to obtain the watermelon rind extract. In a beaker containing 25 mL of 0.1 M $CdCl_2$ solution, 25 mL of freshly prepared watermelon rind extract was added with stirring and to this mixture, freshly prepared 25 mL 0.1 M Na_2S solution was added drop by drop. An orange yellow precipitate started appearing spontaneously upon addition of Na_2S suggesting the formation of CdS compounds. After complete addition of the Na_2S solution, the mixture was stirred continuously for another 30 min in order to ensure that all the Cd^{2+} ions react with S^{2-} ions to form CdS. The mixture was later centrifuged to obtain the CdS nanoparticles and the supernatant solution was discarded. The solid product was stored and subjected to characterization to confirm the formation of the CdS nanoparticles.

Analytical instrumentation

The synthesised CdS nanoparticles were analysed with Bruker D8 Advance powder XRD for obtaining the diffraction peaks. A JEOL JEM 2100F high resolution transmission electron microscope was utilised to visualise the shape and size of the CdS nanoparticles. A double beam UV-Visible spectrophotometer (U-2800, Hitachi) was used to determine the concentrations of the synthetic dyes.

Response surface methodology

The central composite design (CCD) is a second-order polynomial design extensively employed in response surface methodology (RSM), particularly for studying the collective impact of various operational variables on the efficiency of cation adsorption. A notable advantage of CCD in a step-by-step experimental process is its ability to yield meaningful results with a minimal number of designated points. This approach provides a practical framework for data fitting and offers valuable insights that can be effectively utilized to either choose or improve the proposed model. In this study, a full factorial design consisting of 20 runs was conducted, and the main factors,

symbols, and their corresponding values are determined. The CCD was implemented using Design Expert 13 software.

UV-Visible spectrophotometer analysis

In this study, a UV-visible spectrophotometer (U-2800 Hitachi) equipped with a double beam slitter was utilized. The test samples, held in 3 mL quartz glass cuvettes, were subjected to analysis within the UV chamber. For determining Methylene Blue (MB) concentration, the analysis was conducted at 665 nm, while a wavelength of 590 nm was employed for Crystal Violet (CV) estimation. Calibration curves for MB and CV were established using standard solutions of these dyes. The residual concentrations of the dyes were then determined by referencing these calibration curves. The removal efficiency and adsorption capacity of CdS nanoparticles toward MB and CV were calculated using the following equations.

$$\% \, Removal = \frac{(C_0 - C_1)}{C_0} \times 100 \tag{1}$$

$$q_e = (C_0 - C_1)\frac{V}{M} \tag{2}$$

where C_0 is the initial concentration of the adsorbate ions and C_1 is the residual concentration of the adsorbate ions. V is the volume of the solution and M is the mass of the CdS nanoparticles. Q_e is the loading capacity of the CdS nanoparticles synthesised by the aqueous extract of the Watermelon rind.

RESULTS AND DISCUSSION

Watermelon rinds are rich in biomolecules and many studies have suggested the presence of various biomolecules and their potential use in food and diet. Considering their biomolecules potential, an aqueous extract of watermelon rind was prepared and used in the synthesis of CdS nanoparticles as reported in the literature. The biomolecules of watermelon rind act as capping and stabilizing agents in the synthesis of CdS nanoparticles [18].

Characterization of CdS nanoparticles

X-Ray diffraction (XRD) analysis was conducted on CdS nanoparticles synthesized using the watermelon rind extract to validate their crystalline nature (Figure 1). The XRD patterns revealed distinct peaks at 2θ values of 24.86, 26.59, 28.36, 43.71, 47.56, and 51.42, corresponding to the (100), (111), (101), (110), (103), and (112) diffraction planes of hexagonal-structured CdS nanoparticles, in accordance with the JCPDS number 80-0006. The broad nature of these peaks suggests a very small crystallite size. Using the Scherrer formula, the mean crystallite size was calculated to be 15 nm. These findings suggest that watermelon rind extract played a vital role as a stabilizing and capping agent during the synthesis of CdS nanoparticles.

High resolution TEM images of CdS nanoparticles at various magnifications are represented in Figure 2. The investigation on CdS nanoparticles revealed that the CdS are spherical in shape with a size < 10 nm. The biomolecules of watermelon rind extract have capped the CdS nanoparticles and thus stabilised the shape and size of the CdS nanoparticles. The CdS nanoparticles seems to be agglomerated and this is due to the biomolecules coordinating with the neighbouring biomolecules. The EDX patterns of the CdS nanoparticles are presented in Figure 2 The EDX patterns showed only two signals corresponding to S and Cd elements and it suggests that no impurities were present in the synthesised CdS nanoparticles.
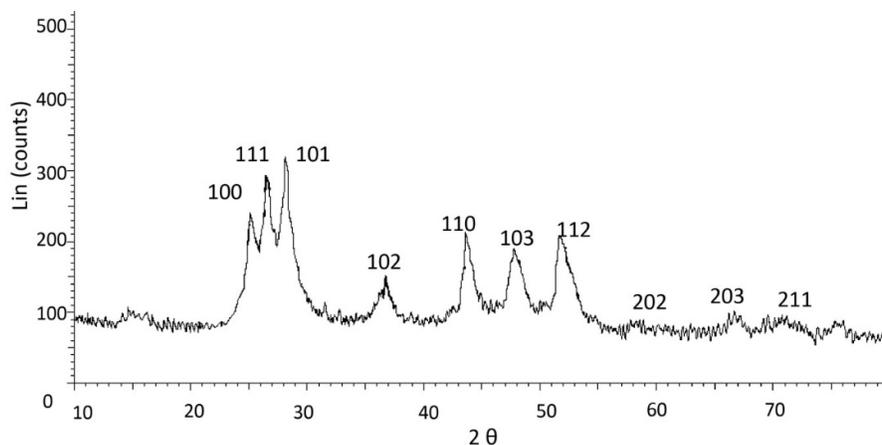
Figure 1. XRD pattern of CdS nanoparticles synthesised using watermelon rind extract.

Response surface methodology

In this research, three independent variables pH, contact time, and initial concentration were selected, and a 20-run central composite design (CCD) was employed. This design comprised 8 cubic points, 6 axial points, and 6 center points within a cube. The predicted and experimental design matrices, along with the analysis of variance for the removal of MB and CV by CdS nanoparticles, are outlined in Tables 2 - 4. The dose of the CdS nanoparticles used in this study is 1.0 gL^{-1} for the MB and CV solutions. A quadratic model was constructed using Design Expert 13, and the second-order polynomial equation describing the removal process is presented in Equation 3 and 4:

% Removal of MB = 78.65 + 6.20 A + 8.68 B – 11.60 C + 1.38 AB -0.87 AC – 2.12 BC – 31.31 A^2 -7.11 B^2 -2.55 C^2 (3)

% Removal of CV = 70.90 + 6.40 A + 8.36 B – 11.30 C + 1.25 AB -1.00 AC – 2.50 BC – 28.86 A^2 -6.69 B^2 -0.65 C^2 (4)

The quadratic equations mentioned earlier are characterized by coefficients that denote their intensity. Moreover, the sign of these coefficients serves as an indicator of whether a specific variable positively or negatively influences the response. A positive coefficient implies that increasing the level of a factor enhances the response, while a negative coefficient suggests that elevating the level of a factor impedes the response. This model encompasses three primary effects, three two-factor interaction effects, and three effects related to curvature. Equation 3 and 4 provides a clear representation of the independent variables and their impact on the responses of the experiment. Furthermore, a close correlation between the experimental and predicted values was observed, suggesting the practicality and improved responses of the experiments. The analysis of variance for the proposed model was analysed and the values are summarised in Table 1 and 2.
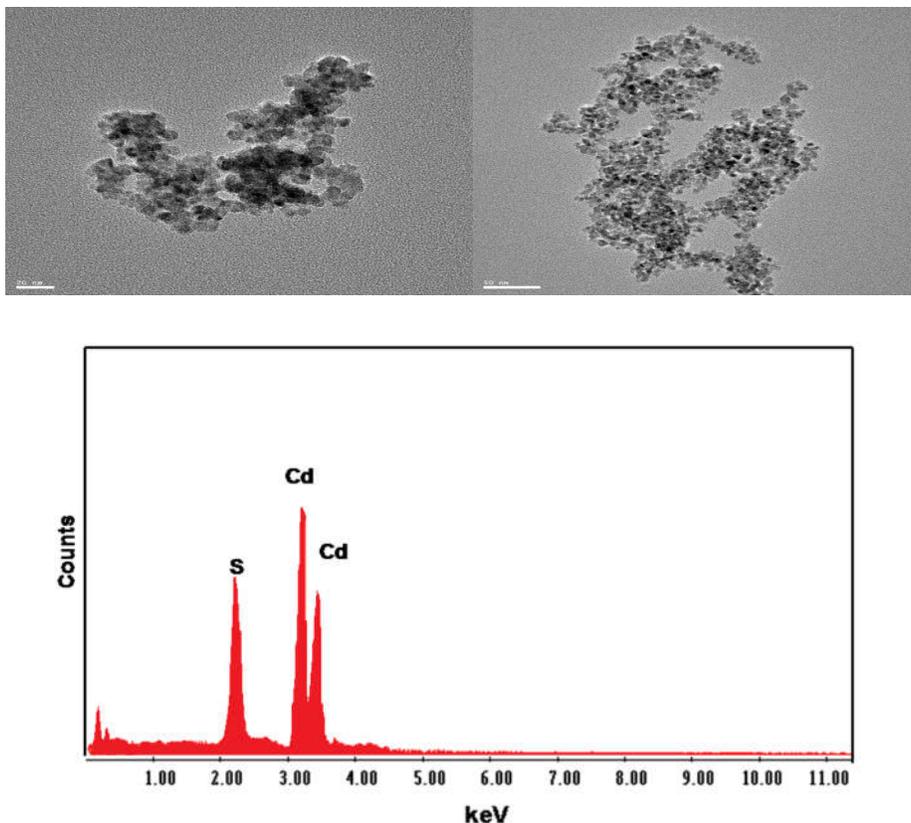
Figure 2. TEM images of CdS nanoparticles synthesised using watermelon rind extract and EDX patterns.

The model's accuracy is substantiated by the remarkably low p-value (<0.0001) and a high F-value (47.85 MB and 35.47 CV), where a low p-value is indicative of statistical significance. In this investigation, the obtained low p-value suggests the significance of the results, underscoring their statistical validity (Table 3 and 4). Additionally, a higher F-value supports the significance of the results and indicates a better fit of the model to the criteria. The lack of fit F-value, found to be >0.005, implies that no systematic variation were encountered in the hypothesized model. High correlation coefficients, approaching 1, indicate a strong alignment between the experimental and predicted values. The adjusted and predicted correlation coefficients were in good agreement with the actual suggesting the appropriateness of the model and its suitability. The adequate precision values were found to be 22.85 and 20.92 respectively for MB and CV suggesting the signals are adequate enough for the models.

To further ensure the adequacy of the adopted model, validation was carried out through a probability plot of actual versus predicted values, assessing the accuracy of the model. As depicted in Figure 3, the plot reveals no significant deviation, affirming the model's reliability. Although a slight scattering of points is observed, the normal distribution of data without any response transformation or issue is implied, as the points align closely with the straight line. This analysis reinforces the robustness and suitability of the proposed model.

Table 1. ANOVA of the quadratic model for the removal of MB by CdS nanoparticles.

Source	Sum of squares	Df	Mean Square	F-value	p-value
Model	13987.96	9	1554.22	47.85	< 0.0001
A-pH	480.50	1	480.50	14.79	0.0032
B-Contact time	1021.39	1	1021.39	31.44	0.0002
C-Initial concentration	1804.25	1	1804.25	55.54	< 0.0001
AB	15.13	1	15.13	0.4656	0.5105
AC	6.13	1	6.13	0.1886	0.6733
BC	36.13	1	36.13	1.11	0.3164
A^2	10082.26	1	10082.26	310.38	< 0.0001
B^2	714.79	1	714.79	22.00	0.0009
C^2	89.18	1	89.18	2.75	0.1285
Residual	324.84	10	32.48		
Lack of Fit	324.00	5	64.80	388.80	0.496
Pure Error	0.8333	5	0.1667		
Cor Total	14312.80	19			
R^2	0.9773				
Adjusted R^2	0.9569				
Predicted R^2	0.8344				
Adeq Precision	22.8542				

Table 2. ANOVA of the quadratic model for the removal of CV by CdS nanoparticles.

Source	Sum of squares	Df	Mean Square	F-value	p-value
Model	12313.28	9	1368.14	35.47	< 0.0001
A-pH	512.00	1	512.00	13.28	0.0045
B-Contact time	947.54	1	947.54	24.57	0.0006
C-Initial concentration	1713.43	1	1713.43	44.43	< 0.0001
AB	12.50	1	12.50	0.3241	0.5817
AC	8.00	1	8.00	0.2074	0.6585
BC	50.00	1	50.00	1.30	0.2814
A^2	8562.82	1	8562.82	222.03	< 0.0001
B^2	633.17	1	633.17	16.42	0.0023
C^2	5.80	1	5.80	0.1505	0.7062
Residual	385.67	10	38.57		
Lack of Fit	383.67	5	76.73	191.83	0.247

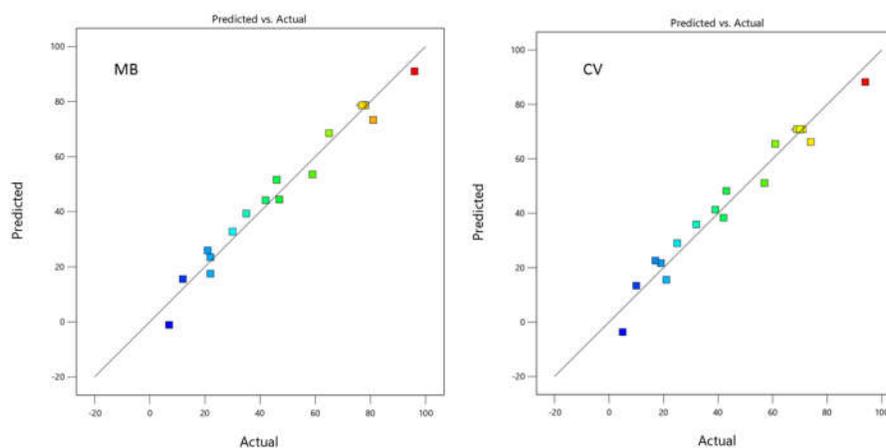| Pure Error	2.00	5	0.4000		
Cor Total	12698.95	19			
R²	0.9696				
Adjusted R²	0.9423				
Predicted R²	0.7793				
Adeq Precision	20.9201				

Figure 3. Probability plot of predicted versus actual obtained for the removal of MB and CV by CdS nanoparticles.

The interactions between two independent variables are visually represented through 3D surface plots, aiding in a better understanding of their correlation and influence on the removal efficiency of MB and CV by CdS nanoparticles. Figures 4 a-c depicts the interaction between two variables while keeping the third variable constant, illustrating the relationship and response of the variables for optimal removal efficiency.

Figure 4a presents a 3D plot of the interaction between pH and contact time and their impact on the percentage removal. The optimal conditions were observed at pH 6 and a contact time exceeding 45 min. A decrease or increase in pH resulted in a decline in removal efficiency, while an increase in contact time led to an enhancement in efficiency, holding initial concentration and adsorbent dosage constant. In the case of the interaction between initial concentration and contact time (Figure 4b), lower concentrations proved to be optimal, requiring a minimum of 45 min to achieve desired results. As the contact time increased, removal efficiency reached a maximum, but efficiency decreased with higher initial concentrations. For the relationship between pH and initial concentration (Figure 4c), the optimal pH was found to be 6 and initial concentration of 50 mg L^{-1}. An increase in initial concentration resulted in a decline in efficiency, suggesting that lower concentrations at pH 6 are highly effective for desirable removal. These 3D surface plots provide valuable insights into the complex interactions and conditions that optimize the removal efficiency of MB and CV by CdS nanoparticles.
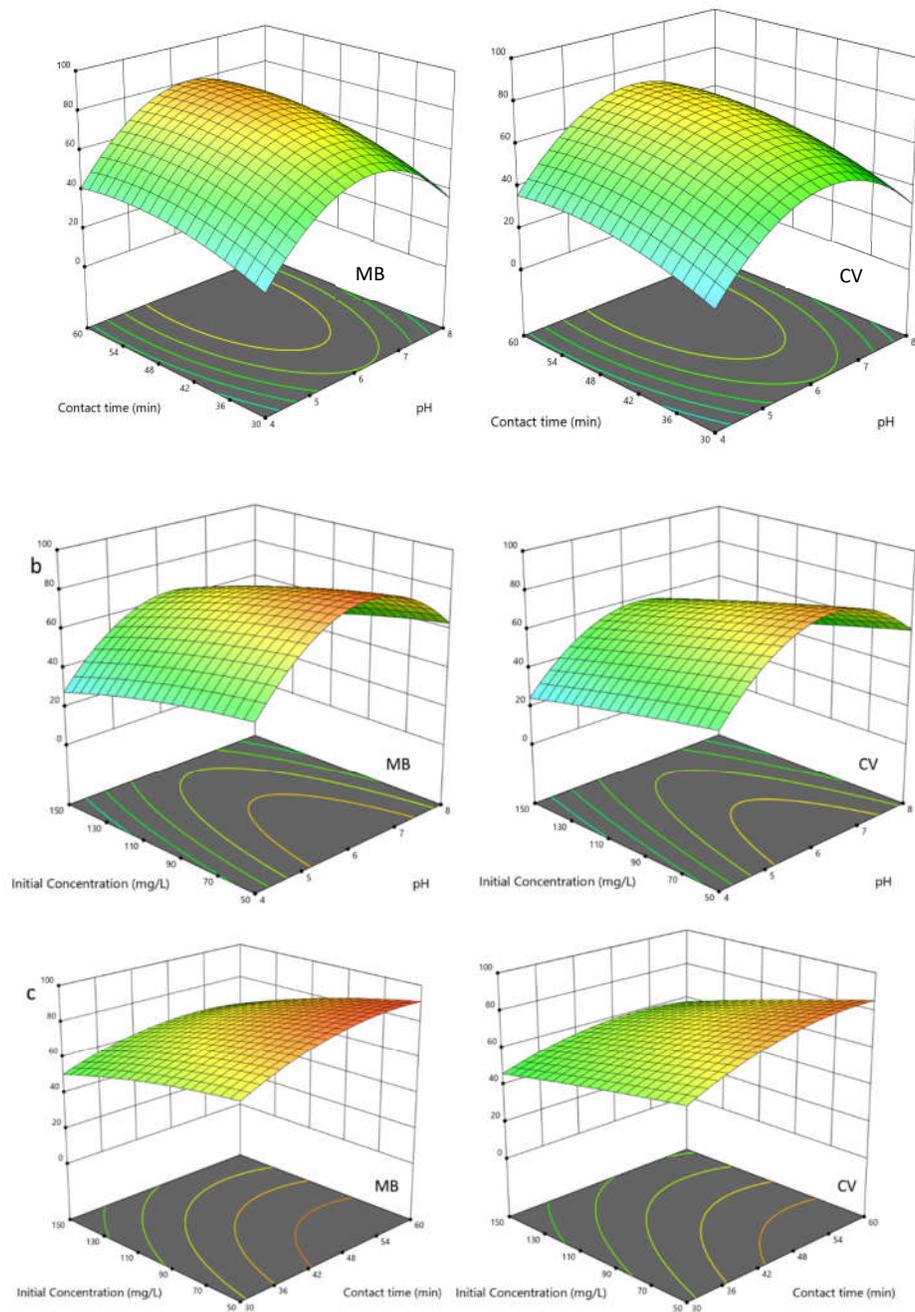
Figure 4. 3D surface plots for the removal of MB and CV by CdS nanoparticles a) contact time vs pH, b) pH vs initial concentration and c) contact time vs initial concentrations.

Adsorption isotherms

Mathematical models play a crucial role in comprehending and validating experimental data, aiding in the understanding of various processes. Numerous models are designed for predicting adsorption processes, with the Langmuir and Freundlich isotherms being among the most frequently utilized ones.

Langmuir isotherm

The Langmuir model stands out as an exemplary mathematical framework that elucidates the monolayer adsorption of an adsorbate onto an adsorbent. It also furnishes the theoretical loading capacity of the adsorbent, facilitating a comparison with experimental values. The linear representation of this equation is as follows:

$$\frac{C_e}{q_e} = \frac{1}{bV_m} + \frac{C_e}{V_m} \tag{5}$$

where C_e is the equilibrium concentration of the adsorbate ions, q_e is the loading capacity of the adsorbent, V_m is the quantity of dye ions at the monolayer and b is the heat of adsorption constant. Experimental data were employed to create plots of C_e/q_e against C_e, and from these plots, the slope and intercept were derived, yielding the constants V_m and b. The Langmuir isotherm constants and correlation coefficients are summarized in Table 3. The results indicate that the equilibrium data obtained for the removal of MB and CV ions by CdS nanoparticles align well with the Langmuir model. The notably high correlation coefficients (0.999 for both MB and CV ions) suggest that the Langmuir model effectively explains the process. Moreover, the agreement between the theoretically calculated loading capacities (227.3 mg L^{-1} for MB and 185.1 mg L^{-1} for CV ions) and the experimental values (225.0 mg L^{-1} for MB and 182.5 mg L^{-1} for CV ions) further substantiates this conclusion. These findings strongly support the assertion that the Langmuir isotherm is the most appropriate model for describing the adsorption of MB and CV ions by CdS nanoparticles, confirming that this adsorption is a monolayer process.

Table 3. Langmuir and Freundlich constants obtained for the removal of MB and CV ions by CdS nanoparticles (dose 1 g/L, temperature 303 K).

Isotherms	Constants	MB	CV
Langmuir	b (L mg^{-1})	0.0066	0.0169
	V_m (mg g^{-1})	227.2	185.1
	R^2	0.999	0.999
Freundlich	K_f	1.918	1.806
	1/n	0.0138	0.0139
	R^2	0.976	0.991

The Langmuir isotherm possesses a distinctive feature expressed through a dimensionless constant, R_L, which provides insights into the favourability or unaffordability of the adsorption process. This dimensionless constant is computed as $R_L = 1 / (1 + bC_0)$, where C_0 is the initial concentration of the adsorbate. If R_L is greater than 1, the adsorption of Methylene Blue (MB) and Crystal Violet (CV) ions by CdS nanoparticles is deemed unfavourable. An R_L value of 1 indicates a linear and irreversible process. For the adsorption to be considered favourable, the condition is $0 < R_L < 1$. If the R_L values fall within the range of 0 to 1, it signifies a favourable adsorption process. The separation factor R_L is expressed mathematically as mentioned above.

The obtained separation factor R_L values for the adsorption of Methylene Blue (MB) and Crystal Violet (CV) ions by CdS nanoparticles reveal that the RL values for both dye ions across various initial concentrations fall within the range of 0 to 1, indicating that the adsorption process is favourable.

Freundlich isotherm

One of the earliest isotherm models utilized for predicting adsorption processes is the Freundlich isotherm model. This model posits the multilayer adsorption of adsorbates onto the surface of adsorbents. The linear equation representing this model is expressed as follows:

$$log\, q_e = log\, K_f + \frac{1}{n} log\, C_e \qquad (6)$$

where q_e is the loading capacity, C_e is the equilibrium concentration of dye ions, K_f is adsorption capacity and n is the intensity of the adsorption.

The equilibrium data derived from the removal of MB and CV ions by CdS nanoparticles were subjected to analysis using the linear equation of the Freundlich isotherm. The constants derived from the Freundlich isotherm are summarized in Table 3. Notably, the correlation coefficients gained for the elimination of MB and CV ions by CdS nanoparticles are close to one, suggesting that the Freundlich model is well-suited for this system, indicating a multilayer adsorption process.

Furthermore, the applicability of the Langmuir isotherm indicates a multilayer process where each layer adheres to the Langmuir isotherm. Consequently, the results suggest that the removal of MB and CV ions by CdS nanoparticles is governed by both Langmuir and Freundlich models.

Kinetics of adsorption

Conducting sorption experiments with variations in the contact time provides valuable insights into the rate-limiting step of the adsorption process and helps discern the underlying adsorption mechanism, whether it is physical or chemical. To address these aspects, kinetic investigations were run by altering the contact time between MB and CV ions and CdS nanoparticles. The obtained data were subjected to verification and analysis using two widely adopted models: the pseudo-first-order (PFO) and pseudo-second-order (PSO) kinetic models. Additionally, the Weber and Morris intraparticle diffusion model was employed to gain a deeper understanding of the adsorption process. The expressions for the PFO and PSO kinetic models are provided below:

$$\ln(q_e - q_t) = \ln q_e - k_1 t \qquad (7)$$

where q_e is the loading capacity at equilibrium and q_t is the loading capacity at different time intervals, t is time and k_1 is the rate constant of pseudo first order.

$$\frac{t}{q_t} = \frac{1}{K_2 q_e^2} + \frac{t}{q_e} \qquad (8)$$

where q_e is the loading capacity at equilibrium and q_t is the loading capacity at different time intervals, t is time and k_2 is the rate constant of pseudo second order.

The PFO and PSO models corresponding constants are summarized in Table 4. Notably, the PFO model demonstrates a poor fit with the kinetic equilibrium data, as evidenced by the low correlation coefficients. Additionally, the theoretical loading capacities of MB and CV ions onto CdS nanoparticles, calculated using the PFO kinetic model, do not align with the experimental values. This incongruence further supports the inadequacy of the model in explaining the kinetic data.

In contrast, the kinetic equilibrium data aligns well with the PSO kinetic model. The robust fit is substantiated by high correlation coefficients close to one for both MB and CV ions (0.999 and 0.998, respectively). Furthermore, the theoretical loading capacities calculated using the PSO model closely match the experimental values, reinforcing the suitability of this model for the present system. The applicability of the PSO model propounds that the rate-limiting step involves chemical reactions governed by the transfer of electrons. However, it is essential to note that meeting specific conditions is necessary to conclusively determine that chemical reactions at the

surface are the rate-limiting step; in many cases, the process tends to be physio-sorption, despite the applicability of the PSO model [19, 20].

Table 4. Kinetic constants of pseudo first and second order for the removal of MB and CV ions by CdS nanoparticles (Dose-1 g/L, Temp 303K).

Kinetic model	Parameters	MB	CV
Pseudo first order	k_1 (min^{-1})	0.014	0.007
	q_e (mg g^{-1})	7.90	9.65
	R^2	0.8707	0.967
Pseudo second order	k_2 (g mg^{-1} min^{-1})	0.021	0.019
	q_e (mg g^{-1})	120.9	117.5
	R^2	0.999	0.998

Thermodynamics of adsorption

In industrial effluents, temperatures typically range from moderate to high due to various processes, and this temperature can significantly influence the adsorption process. Therefore, it is essential to optimize the temperature of the solution to achieve maximum removal or adsorption efficiency. Consequently, in this study, temperature optimization was carried out by varying the temperature for the removal of MB and CV ions by CdS nanoparticles within the range of 303 K to 323 K.

Thermodynamic studies can offer valuable insights into the change in free energy (ΔG), entropy (ΔS), and enthalpy (ΔH) of the adsorption process. To determine these thermodynamic parameters, the following equations were employed:

$$K_D = \frac{q_e}{c_e} \tag{9}$$

$$\Delta G° = -RT \, lnK_D \tag{10}$$

$$\Delta G° = \Delta H° - T\Delta S° \tag{11}$$

$$lnK_D = \frac{\Delta S°}{R} - \frac{\Delta H°}{RT} \tag{12}$$

where K_D is the equilibrium constant, R is gas constant and T is temperature.

The thermodynamic constants derived for the removal of MB and CV ions by CdS nanoparticles are summarized in Table 5. Notably, the values of the change in free energy (ΔG) are consistently negative for both metal ions at various temperatures. This negativity indicates that the elimination of MB and CV ions by CdS nanoparticles is a spontaneous process. Furthermore, it is observed that as the temperature increases, the negative ΔG values decrease, implying a reduction in spontaneity with a rise in temperature. Consequently, both the loading capacity and efficiency of removal also decline with surging temperature.

The enthalpy (ΔH) values are negative for both MB and CV ions, suggesting that the process is exothermic, and heat is released during the adsorption process. This release of heat implies an increase in randomness among the MB and CV ions. The positive values of entropy (ΔS) for both MB and CV ions indicate an increase in randomness and disorderliness with a rise in temperature, which is consistent with the negative enthalpy. Overall, the thermodynamic investigations suggest that the elimination of MB and CV ions by CdS nanoparticles is spontaneous at low temperatures.

Table 5 Thermodynamic parameters of adsorption of MB and CV ions by CdS nanoparticles.

Metal ions	Temperature (K)	Free energy (ΔG)	Enthalpy (ΔH)	Entropy (ΔS)
Pb^{2+}	303	-5135.6	-1326.1	1082.8
	313	-4903.4		
	323	-4769.3		
Cd^{2+}	303	-4384.4	-1122.5	1019.6
	313	-4152.4		
	323	-4033.2		

Regeneration and reusability

Regeneration and reusability are imperative in adsorption based wastewater treatment process. Since the economic aspects of the treatment process can be determined by the regeneration and reusability potential of the CdS nanoparticles. In view of the above, the CdS nanoparticles loaded with MB and CV were investigated for the regeneration efficiency with acids and bases. Acids such as HCl and CH_3COOH and bases such as NaOH and $NaCO_3$ were employed for the investigations and it is found that the acids exhibited superior regeneration efficiency compared to the bases. Further, inorganic acid exhibited higher regeneration compared to organic acid. Hence, 0.01 M HCl was used as desorbing agents and the regenerated CdS nanoparticles were subjected to consecutive adsorption-desorption cycles and it is found that CdS nanoparticles are proficient for 5 cycles without any loss in their efficiencies.

Table 6. Loading capacity comparison of CdS nanoparticles with other adsorbents.

S.No	Adsorbent	Dye	Loading capacity ($mg\ g^{-1}$)	Reference
1	Fe3O4@PDA/HKUST-1	MB	34.0	[21]
2	BiVO4 hollow cuboids	MB	74.11	[22]
3	Metal-polyphenol networks	CV	40.48	[23]
4	Sugarcane Bagasse	MB	112.9	[24]
		CV	107.5	
5	Leaves of Ficus Benjamina	MB	25.3	[25]
		CV	11.01	
6	MgO/graphene oxide composite	MB	171.9	[26]
7	Geopolymer	MB	87.82	[27]
8	Zero-valent iron	CV	172.4	[28]
		MB	151.5	
9	Activated Carbon	MB	123.7	[29]
		CV	120	
10	Industrial microbial waste	CV	175.4	[30]
		MB	92.6	
11	Calix[8]arene-PbS nano	MB	45.0	[31]
12	Cu-CNFs	MB	165.0	[32]
13	Hydrogel Cross-linked N-maleyl chitosan	MB	66.89	[33]
		CV	64.56	
14	Polyacrylonitrile composite nanofiber	MB	128.2	[34]
15	CNT-Polyacrylonitrile composite nanofiber	MB	158.7	
16	CdS nanoparticles	MB	225.0	This study
		CV	182.5	

Comparison of loading capacities

The loading capacities of adsorbents play a crucial role in determining their efficiency, making them a primary consideration for selection in industrial treatment processes. In this study, the loading capacity of CdS nanoparticles was determined to be 225.0 mg g^{-1} for Methylene Blue (MB) ions and 182.5 mg g^{-1} for Crystal Violet (CV) ions. Notably, the adsorption capacity of MB was found to be higher than that of CV, a difference that can be attributed to the molecular structures of the two dyes. The molecular structure of MB is smaller and simpler compared to the larger and more complex structure of CV. The smaller and linear size of MB ions allows for easy diffusion into the pores of CdS nanoparticles, and they can readily bind to active sites through electrostatic attraction. On the other hand, the larger molecular size of CV may encounter steric hindrance during pore diffusion and binding to active sites. To evaluate the efficiency of CdS nanoparticles, their loading capacities were compared with those of other adsorbents reported in the literature. A summary of this comparison is presented in Table 6. It is noteworthy that the loading capacities of CdS nanoparticles towards both MB and CV ions were found to surpass those of several adsorbents reported in the literature.

CONCLUSION

This study delved into the efficacy of CdS nanoparticles in removing Methylene Blue (MB) and Crystal Violet (CV) ions from aqueous solutions. A CCD was developed to optimise the independent variables and the developed model was found to be reliable and robust for the removal of MB and CV by CdS nanoparticles. The p-value and lack of fit was found to be significant with adequate precision. The equilibrium data were scrutinized using mathematical models, revealing a multilayer adsorption mechanism where each layer adheres to the Langmuir isotherm. Kinetic data analysis indicated adherence to a pseudo-second-order kinetic model, suggesting that chemical reactions govern the rate-limiting step. Thermodynamic investigations disclosed the spontaneity and exothermic nature of the entire process, particularly at lower temperatures. Desorption studies demonstrated the remarkable reusability of CdS nanoparticles across successive cycles. Consequently, CdS nanoparticles synthesized through the green synthesis method emerged as superior adsorbents, showcasing significant potential for practical applications.

REFERENCES

1. Rai, P.K. An eco-sustainable green approach for heavy metals management: two case studies of developing industrial region. *Environ. Monit. Assess*. **2012**, 184, 421-448.
2. Arora, N.K.; Chauhan, R. Heavy metal toxicity and sustainable interventions for their decontamination. *Environ. Sustain*. **2021**, 4, 1-3.
3. Peng-Song, L.; Hu-Chun, T. Cell surface engineering of microorganisms towards adsorption of heavy metals. *Crit. Rev. Microbiol.* **2015**, 41, 140-149
4. Sahmoune, M.N. Evaluation of thermodynamic parameters for adsorption of heavy metals by green adsorbents. *Environ. Chem. Lett.* **2019**, 17, 697-704.
5. Khulbe, K.C.; Matsuura, T. Removal of heavy metals and pollutants by membrane adsorption techniques. *Appl. Water Sci.* **2018**, 8, 19.
6. Mariana, M.; Khalil, H.P.S.A.; Mistar, E.M.; Yahya, E.B.; Alfatah, T.; Danish, M.; Amayreh, M. Recent advances in activated carbon modification techniques for enhanced heavy metal adsorption. *J. Water Process. Eng.* **2021**, 43, 102221.
7. Lakshmipathy, R.; Sarada, N.C.; Jayaprakash. N. Agricultural wastes as low cost adsorbents for sequestration of heavy metal ions and synthetic dyes from aqueous solution: A mini review. *Int. J. ChemTech Res.* **2015**, 8, 25-31.

8. Soliman, N.K.; Moustafa, A.F. Industrial solid waste for heavy metals adsorption features and challenges; a review. *J. Mater. Res. Technol.* **2020**, 9, 10235-10253.

9. Isaac, P.J.; Sivakumar, A.; Kamil, M.S.M.; Cheralathan, K.K.; Lakshmipathy, R. Synthesis of zeolite/activated carbon composite material for the removal of lead(II) and cadmium(II) ions. *Environ. Prog. Sustain. Energy* **2019**, 38, e13246.

10. Natale, F.D.; Gargiulo, V.; Alfè, M. Adsorption of heavy metals on silica-supported hydrophilic carbonaceous nanoparticles (SHNPs). *J. Hazard. Mater.* **2020**, 393, 122374.

11. Ekrami, E.; Pouresmaieli, M.; Hashemiyoon, E.S.; Noorbakhsh, N.; Mahmoudifard, M. Nanotechnology: A sustainable solution for heavy metals remediation. *Environ. Nanotechnol. Monit. Manag.* **2022**, 18, 100718.

12. Hassan, K. Heavy metal removal from water by magnetite nanorods. *Chem. Eng. J.* **2013**, 219, 209-216.

13. Chi, H.N.; Ruey-Shin J. Efficient removal of cationic dyes from water by a combined adsorption-photocatalysis process using platinum-doped titanate nanomaterials. *J. Taiwan Inst. Chem. Eng.* **2019**, 99, 166-179.

14. Hala, R.M,; Shaimaa, M.I,; Sahar A.E. Textile dye removal from aqueous solutions using cheap MgO nanomaterials: Adsorption kinetics, isotherm studies and thermodynamics. *Adv. Powder Technol.* **2016**, 27, 223-231.

15. Ruba, M.; Ali, K.; Naqvi, S.A.Z.; Maqsood, M.A.; Bashir, M.Z.; Noreen, S. Biosynthesis of *Leucaena leucocephala* leaf mediated ZnO, CuO, MnO2, and MgO based nano-adsorbents for Reactive Golden Yellow-145 (RY-145) and Direct Red-31 (DR-31) dye removal from textile wastewater to reuse in agricultural purpose. *Sep. Purif. Technol.* **2023**, 306, 122527.

16. Amin, R.M.; Mahmoud, R.K.; Gadelhak, Y.; Abo El-Ela, F.I. Gamma irradiated green synthesized zero valent iron nanoparticles as promising antibacterial agents and heavy metal nano-adsorbents. *Environ. Nanotechnol. Monit. Manag.* **2021**, 16, 100461.

17. Janani, R.; Gurunathan, B.; Sivakumar, K.; Varjani, S.; Ngo, H.H.; Gnansounou, E. Advancements in heavy metals removal from effluents employing nano-adsorbents: Way towards cleaner production. *Environ. Res.* **2022**, 203, 111815.

18. Lakshmipathy, R.; Sarada, N.C.; Chidambaram K.; Basha, S.K. One step low temperature fabrications of CdS quantum dots by watermelon rind: Green approach. *Int. J. Nanomed.* **2015**, 10, 183-188.

19. Serap, F. Adsorption of diazo dye direct red-28 and tetra-azo dye direct black-22 using calcined kaolin in aqueous solutions. *Bull. Chem. Soc. Ethiop.* **2023**, 37, 593-610.

20. Fatma E.T.; Raziye K. Investigation of lead removal from aqueous solutions using modified natural clay: Kinetics and thermodynamics approaches. *Bull. Chem. Soc. Ethiop.* **2023**, 37, 231-244.

21. Gang, Z.; Qi, W.; Ruixin, S.; Shuailong, L.; Siao, Y.; Qi, Z. Synthesis of core-double-shell structured Fe_3O_4@PDA/HKUST-1: Characterization analysis and adsorption performance on cationic MB dyes. *J. Phys. Chem. Solids* **2023**, 172, 111094.

22. Qianfei, M.; Jinyuan, M.; Zhansheng, L.; Kanghui, Y.; Zao, Y.; Xianwen, W.; Xiujuan, C.; Hua, Y. Experimental and theoretical elucidation of adsorption performance and mechanism of surface-engineered $BiVO_4$ hollow cuboids for removing MB and other pollutants. *J. Mol. Liq.* **2023**, 373, 121234.

23. Mingkun, G.; Donghui, X.; Yuhang, G.; Ge, C.; Rongqi, Z.; Xiaodong, H.; Xiaomin, X.; Jing, W.; Xin, Y.; Guangyang, L. Mussel-inspired triple bionic adsorbent: Facile preparation of layered double hydroxide@polydopamine@metal-polyphenol networks and their selective adsorption of dyes in single and binary systems. *J. Hazard. Mater.* **2021**, 420, 126609.

24. Alaa, S.O.; Gamal, A.N.; Abd-Elhamid, A.I.; Omaima, O.M.F.; El-Bardan, A.A.; Hesham, M.A.S.; Nayl, A.A. Adsorption of crystal violet and methylene blue dyes using a cellulose-based adsorbent from sugercane bagasse: Characterization, kinetic and isotherm studies. *J. Mater. Res. Technol.* **2022**, 19, 3241-3254.

25. Varuna, W.; Sunil, K.; Preeti, K. Development of dried uncharred leaves of *Ficus benjamina* as a novel adsorbent for cationic dyes: Kinetics, isotherm, and batch optimization. *Ind. Crops Prod.* **2023**, 195, 116449.

26. Ting, G.; Chaoke, B. Facile fabrication of MgO/graphene oxide composite as an efficient adsorbent for rapid removal of aqueous organic dyes: Performance evaluation and mechanistic investigation. *J. Phys. Chem. Solids* **2021**, 158, 110251.

27. Janani, K.; Mullaimalar, A.; Jeyalakshmi, R. Adsorption of dyestuff by nano copper oxide coated alkali metakaoline geopolymer in monolith and powder forms: Kinetics, isotherms and microstructural analysis. *Environ. Res*. **2023**, 218, 115002.

28. Jiwei, L.; Yongmei, W.; Yi, F.; Teza, M.; Shaoxian, S.; Changsheng, P. Removal of crystal violet and methylene blue from aqueous solutions using the fly ash-based adsorbent material-supported zero-valent iron. *J. Mol. Liquid* **2018**, 250, 468-476.

29. Mariam, S.G.; Abd-Elhamid, A.I.; El-Shanshory, A.A.; Hesham M.A.S. Adsorption of cationic dyes onto chemically modified activated carbon: Kinetics and thermodynamic study. *J. Mol. Liquid* **2022**, 346, 118227

30. Jiayang, L.; Fujia, C.; Chunzhi, L.; Leizhen, L.; Changwei, H.; Yu, Wei.; Paul, R.; Qingguo, H. Characterization and utilization of industrial microbial waste as novel adsorbent to remove single and mixed dyes from water. *J. Clean. Prod.* **2019**, 208, 552-562.

31. Nor, Z.R.; Syahirah, I.; Abdul, H.A.; Mazliana, A.K.; Siti, E.A.; Shahrul, A.A.A. Fabrication and optimization calix[8]arene-PbS nanoadsorbents for the adsorption of methylene blue: Isotherms, kinetics and thermodynamics studies. *J. Saudi Chem. Soc.* **2022**, 26, 101402.

32. Justin, K.G.; Nishith, V.; Bhaskar, B. Hydrophilic graphitic carbon nitride-supported Cu-CNFs: An efficient adsorbent for aqueous cationic dye molecules. *Mater. Lett.* **2021**, 294, 129762.

33. Mahdi, T.M.; Gholam, B.M.; Mehran, K. Poly(AA-co-VPA) hydrogel cross-linked with N-maleyl chitosan as dye adsorbent: Isotherms, kinetics and thermodynamic investigation. *Int. J. Biol. Macromol.* **2018**, 117, 152-166.

34. Dem, Y.; Şerife, P. Carbon nanotubes/ polyacrylonitrile composite nanofiber mats for highly efficient dye adsorption. *Colloids Surf. A Physicochem. Eng. Asp*. **2022**, 651, 129703.